

# Critical current for giant Fano factor in neural models with bistable firing dynamics and implications for signal transmission

Richard Kullmann,<sup>1,2</sup> Gregory Knoll<sup>1,2</sup>, Davide Bernardi<sup>3</sup> and Benjamin Lindner<sup>1,2</sup>

<sup>1</sup>*Bernstein Center for Computational Neuroscience Berlin, Philipstrasse 13, Haus 2, 10115 Berlin, Germany*

<sup>2</sup>*Physics Department of Humboldt University Berlin, Newtonstrasse 15, 12489 Berlin, Germany*

<sup>3</sup>*Center for Translational Neurophysiology of Speech and Communication, Fondazione Istituto Italiano di Tecnologia, via Fossato di Mortara 19, 44121 Ferrara, Italy*

(Received 8 September 2020; revised 29 August 2021; accepted 5 January 2022; published 25 January 2022)

Bistability in the firing rate is a prominent feature in different types of neurons as well as in neural networks. We show that for a constant input below a critical value, such bistability can lead to a giant spike-count diffusion. We study the transmission of a periodic signal and demonstrate that close to the critical bias current, the signal-to-noise ratio suffers a sharp increase, an effect that can be traced back to the giant diffusion and large Fano factor.

DOI: [10.1103/PhysRevE.105.014416](https://doi.org/10.1103/PhysRevE.105.014416)

## I. INTRODUCTION

The stochasticity encountered in transport and diffusion processes in statistical physics has, at first glance, little to do with the stochasticity of spiking nerve cells that may encode information about sensory stimuli. However, there are striking analogies between the statistical characteristics of both phenomena. The position and mean velocity of a Brownian particle are equivalent to the spike count and firing rate of a spiking neuron, respectively: the spike count  $N(t_0, t)$  in the time window  $(t_0, t)$  can be regarded as a one-sided random walk, i.e., a kind of discrete position variable, and the temporal derivative of its ensemble average, i.e., the firing rate  $r(t) = \langle N(t, t + \Delta t) \rangle / \Delta t$ , can be seen as the mean velocity. The particle's diffusion coefficient and Péclet number have their counterpart in the spike-count diffusion coefficient and the (inverse) Fano factor, characterizing the variability (or, equivalently, the regularity) of the transport or the spike generation, respectively. These analogies (summarized in Fig. 1) are fruitful because we may ask what certain nontrivial statistical phenomena observed in one class of models may imply for the other.

For active particles that switch between two directions of motion [1], for assemblies of molecular motors that show a similar bistability in their velocity [2–6], and for underdamped particles in a periodic potential that switch stochastically between a bound and a running state [7–10], it has been shown that the diffusion coefficient grows exponentially with a shrinking amplitude of the driving fluctuations if the asymmetry between the two velocity states is not too strong.

There are similar bistabilities between two firing states in some types of neurons, such as pacemaker neurons [11], sensory neurons [12], and motoneurons [13], which are also suggested to play important roles in short-term memory and information processing [12,14] as well as in shaping patterns

of so-called spindle oscillations [15]. Likewise, at the neural network level, there are population-wide transitions between up and down states [16–18], a kind of bistability in the population rate with substantial implications for signal processing [19–21]. Theoretical studies have revealed several mechanisms for generating such bistability, ranging from generic networks of spiking neurons with adaptation and/or synaptic dynamics (e.g., in [22–25]) and rate models with traveling waves (e.g., in [24,26]) to the more abstract but general framework of self-organized bistability [27,28].

From the viewpoint of nonlinear dynamics, these neural systems show two attractors in phase space: a stable limit cycle and a stable resting state; in the presence of fluctuations, transitions between these states are observed. Focusing on the

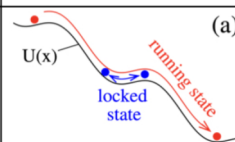
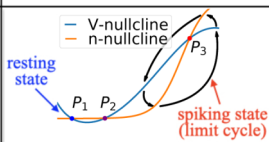
transport model	neuron model
	
position, phase	spike count
mean velocity	firing rate
diffusion coefficient	Fano factor x rate
Velocity power spectrum	Spike train power spectrum
temperature	inverse number of channels

FIG. 1. Analogies between the mechanical transport model and the neuron model. The table illustrates the correspondence of characteristics of the transport model and the (single) neuron model.

single-neuron example, we can thus conjecture that the spike count in a bistable neuron can display the same giant diffusion as observed, e.g., for underdamped particles in a suitably tilted periodic potential. Consequently, we may expect that within an input range limited by a *critical current*, the variability of the spike count will increase drastically with decreasing noise. Here we pursue this question in terms of the diffusion coefficient, but we also study the behavior of the Fano factor (a more common measure of spiking variability in computational neuroscience), and we explore the consequences of giant spike-count diffusion for the transmission of a weak periodic signal. We demonstrate that (i) the specific form of firing bistability (the bifurcation by which the bistability emerges as well as whether it is at the single-neuron level or at the network level) does not matter for the effect; (ii) the two-state theory developed for the transport models can be applied to neural systems with firing-rate bistability and extended to the case of periodic driving to capture salient features of signal transmission; and (iii) the concept of a critical asymmetry determines a value of the neural input current at which the signal-to-noise ratio undergoes a drastic increase; our theory elucidates the causal relationship between this effect and the properties of the transition rates. We show this in models of a single neuron and of a bistable network.

## II. TWO NEURONS WITH SPIKE-RATE BISTABILITY

We study a version of the  $I_{Na,p} + I_K$  model, a two-dimensional simplification of the Hodgkin-Huxley model popularized by Izhikevich [29], containing additive noise:

$$\begin{aligned} C\dot{V} &= I - g_L(V - E_L) - g_{Na}m_\infty(V)(V - E_{Na}) \\ &\quad - g_Kn(V - E_K) + \sqrt{2D}\xi(t), \\ \dot{n} &= [n_\infty(V) - n]/\tau(V). \end{aligned} \quad (1)$$

Here  $V$  denotes the membrane voltage,  $C$  is the capacitance,  $I$  is the bias current,  $g_i$  are conductances, and  $E_i$  are the Nernst equilibrium potentials. Noise with intensity  $D$  accounts for the observed neural variability and can be caused by channel fluctuations, stochastic input from other neurons, and synaptic variability (for another version of this model, in which channel noise is incorporated in more detail, see [30]). The function  $m_\infty(V)$  represents the activation of the instantaneous  $Na^+$  current, while  $n$  is a slower dynamical variable describing the fraction of open  $K^+$  channels. Following [29], all steady-state activation functions are approximated by sigmoid functions of the type  $f_\infty(V) = [1 + \exp\{(V_{1/2} - V)/k\}]^{-1}$ .

Two sets of parameters were chosen such that bistability of the firing rate emerges either through a saddle-node bifurcation off invariant circle (see Fig. 2) or a subcritical Andronov-Hopf bifurcation (see Fig. 3). Simulations were carried out using the Euler-Maruyama method with time steps of  $5 \times 10^{-4}$  and  $5 \times 10^{-3}$  ms for the saddle-node and Andronov-Hopf cases, respectively. Data were obtained from 50 trials that were simulated for  $5 \times 10^{10}$ – $10^{11}$  time steps.

Typical features of spiking bistability are illustrated in the system with a stable-node resting state in Fig. 2. For a small value of injected current  $I$  [Fig. 2(a)], the system resides either in a lower quiescent state or in a higher-baseline spiking state [the spikes are magnified in Fig. 2(c)]. Increasing the input

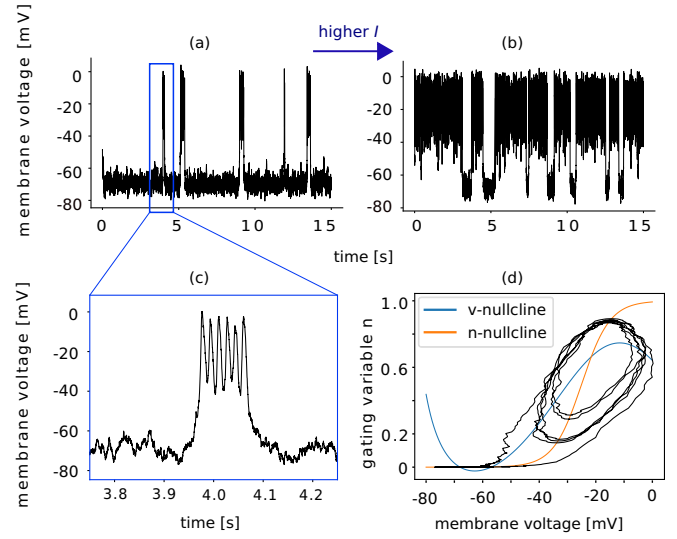


FIG. 2. Firing bistability in the  $I_{Na,p} + I_K$  model with saddle-node bifurcation. (a),(b) Membrane voltage for two different bias currents as a function of time [a magnified version of (a) in (c) reveals single action potentials in the spiking state]. In the phase plane of the system (d), the quiescent state corresponds to a stable node, while the spiking state corresponds to a stable limit cycle (two transitions between these states are shown). Parameters are as follows:  $C = 1 \mu A/cm^2$ ,  $g_L = 0.3 mS/cm^2$ ,  $E_L = -80 mV$ ,  $g_{Na} = 1 mS/cm^2$ ,  $E_{Na} = 60 mV$ ,  $g_K = 0.4 mS/cm^2$ ,  $E_K = -90 mV$ ,  $k_m = 14 mV$ ,  $V_{1/2,m} = -18 mV$ ,  $k_n = 5 mV$ ,  $V_{1/2,n} = -25 mV$ , and  $\tau(V) = \text{const} = 3 ms$ .

current results in more frequent and longer-lasting spiking [Fig. 2(b)]. The mechanism for the bistability can be understood in terms of the nullclines with their three intersection points (stable node, saddle point, and unstable focus) shown in Fig. 2(d). In this configuration, the system either displays small-scale fluctuations around the stable node (corresponding to the quiescent state) or continuous rotations around the unstable focus (corresponding to the spiking state), and transitions between those states are enabled by noise-induced fluctuations. We identify the subsequent passing of two critical lines around the unstable focus as the emergence of a

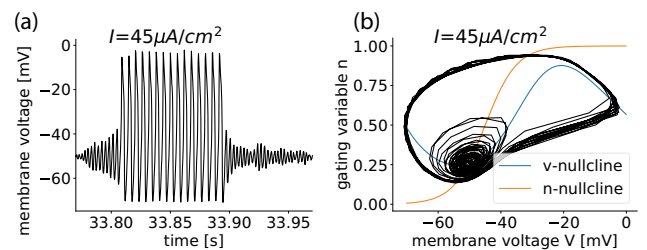


FIG. 3.  $I_{Na,p} + I_K$  model with subcritical Andronov-Hopf bifurcation. Evolution of the membrane voltage over time (a) and the corresponding trajectory in the phase plane (b). Small fluctuations correspond to the resting state, and strong oscillations indicate the spiking state. Parameters are as follows:  $C = 1 \mu A/cm^2$ ,  $g_L = 1 mS/cm^2$ ,  $E_L = -78 mV$ ,  $g_{Na} = 4 mS/cm^2$ ,  $E_{Na} = 60 mV$ ,  $g_K = 4 mS/cm^2$ ,  $E_K = -90 mV$ ,  $k_m = 7 mV$ ,  $V_{1/2,m} = -30 mV$ ,  $k_n = 5 mV$ ,  $V_{1/2,n} = -45 mV$ , and  $\tau(V) = \text{const} = 1 ms$ .

spike, and the instant in time of the crossing of the first line is registered as the time  $t_i$  of the  $i$ th spike.

With the second parameter set, illustrated in Fig. 3, the  $I_{Na,p} + I_K$  model exhibits bistability in the amplitude of its oscillations around a single fixed point: the quiescent state is characterized by small-amplitude fluctuations around the equilibrium point, while the spiking state shows large-amplitude oscillations around the same point. Still, changes in the input current have the same effects as above: small and large values favor the resting and spiking state, respectively. In this setting, we count as a spike only oscillations with an amplitude above a threshold.

### III. GIANT DIFFUSION OF THE SPIKE COUNT

Here we consider an abstract spike train of  $\delta$  functions,  $x(t) = \sum \delta(t - t_i)$ , and its integral, the count variable  $N(t) = \int_0^t dt' x(t')$ . We define the firing rate as the ensemble average  $r = \langle x(t) \rangle$  of the spike train, and we quantify the variability of the spike count by its effective diffusion coefficient  $D_{\text{eff}}$  and by the asymptotic Fano factor  $F$ ,

$$D_{\text{eff}} = \lim_{t \rightarrow \infty} \frac{\langle [N(t) - \langle N(t) \rangle]^2 \rangle}{2t},$$

$$F = \lim_{t \rightarrow \infty} \frac{\langle [N(t) - \langle N(t) \rangle]^2 \rangle}{\langle N(t) \rangle}. \quad (2)$$

When calculating these statistics in practice, it is important to ensure that the time window  $t$  and averaging ensemble are sufficiently large in order to avoid introducing a systematic bias in the Fano factor [31,32]. While the diffusion coefficient underpins the analogy to the stochastic motility models [1,7,33,34], the Fano factor is a measure of spike variability used more often in the field of computational neuroscience [31,35–38] with the simple reference value for a Poisson process of  $F = 1$ .

#### A. Simulation results

In Fig. 4 we show results for the count statistics (firing rate, diffusion coefficient, and Fano factor) in both bifurcation regimes [saddle-node in (a) and Andronov-Hopf in (b)] and for different noise intensities as indicated. Looking at the top panels, the firing rates behave quite regularly: they increase with  $I$ , and for large  $I$  they approach the deterministic firing rate on the limit cycle (black line); the dependence becomes less steep for larger noise intensities, but this is not a very drastic effect. The diffusion coefficient and the Fano factor (mid and lower panels, respectively), however, show a nonmonotonic behavior, both passing through maxima. A lower noise intensity results in a steeper dependence for all these firing characteristics versus input current. Notably, the diffusion coefficient and Fano factor at a low noise intensity undergo dramatic changes spanning orders of magnitude when  $I$  is varied over the shown range. In particular, we recover the finite range of diverging diffusion coefficients observed in models of active [3] and underdamped passive Brownian motion [7–10], i.e., diffusion curves for different noise levels (approximately) intersect at two critical values of the input current. Most remarkably, at the higher of these two critical values, the Fano factors also intersect: below this value

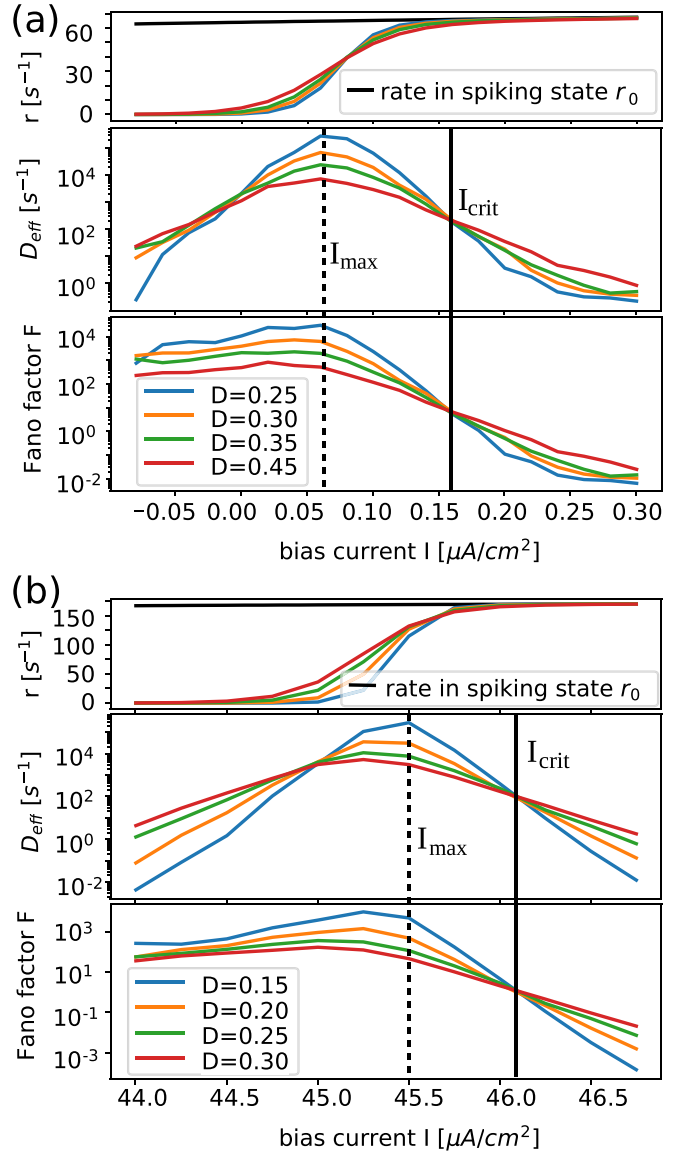


FIG. 4. Count statistics as a function of  $I$  of the  $I_{Na,p} + I_K$  model. From top to bottom: overall firing rate, effective diffusion coefficient, and Fano factor for  $I_{Na,p} + I_K$  model with saddle-node bifurcation (a) and with subcritical Andronov-Hopf bifurcation (b). Note that for  $D = 0$  the bifurcations to stable tonic firing would occur outside the shown ranges at  $I \approx 0.36 \mu\text{A}/\text{cm}^2$  and  $I \approx 48.9 \mu\text{A}/\text{cm}^2$  in (a) and (b), respectively.

$I_{\text{crit}}$ , the Fano factor increases strongly with decreasing noise intensity  $D$ ; above it ( $I > I_{\text{crit}}$ ) the Fano factor drops strongly with decreasing  $D$ . We would like to emphasize that all of these observations can be made both for the system close to a saddle-node bifurcation off the invariant circle [Fig. 4(a)] and for the system close to an Andronov-Hopf bifurcation [Fig. 4(b)].

#### B. Two-state theory

In the case of low noise intensity, the transition times between the resting state and the firing state will be much shorter than the periods of time that the neuron stays in either

state, allowing for a concise description of the system in terms of two discrete states  $R$  (for resting) and  $F$  (for firing). The transition rates between the states are assumed to obey an Arrhenius law:

$$\nu_X = \nu_{0_X} \exp\left(-\frac{\Delta U_X}{D}\right), \quad X \in \{R, F\}, \quad (3)$$

where  $\nu_X$  denotes the transition rate from state  $X$  to the respective other state,  $\Delta U_X$  is the corresponding potential barrier that needs to be overcome, and  $D$  is the noise intensity. By fitting the rates for a given input current to different levels of noise, we can determine  $\Delta U_X(I)$ , similar to the procedure done in Ref. [7]. For a similar approach to describing the ISI statistics in bistable neurons, see [39].

An elementary calculation shows that the probability to be in the firing state is  $\nu_R/(\nu_F + \nu_R)$ , and, if  $r_F$  is the firing rate in the firing state, the overall firing rate will be  $r_F \nu_R/(\nu_F + \nu_R)$ . The growth over time of the spike count variance follows from the integral over the velocity's exponential autocorrelation function via the Kubo theorem. Summarizing the results, we get the following formulas for the stationary firing rate, the diffusion coefficient, and the Fano factor of the spike count:

$$r = r_F \frac{\nu_R}{\nu_F + \nu_R}, \quad D_{\text{eff}} = \frac{r_F^2 \nu_F \nu_R}{(\nu_F + \nu_R)^3}, \quad F = \frac{2r_F \nu_F}{(\nu_F + \nu_R)^2}. \quad (4)$$

For more details on the general problem, see [3] and the discussion of the related problem of Taylor dispersion by Van den Broeck [33].

We have measured the rates as functions of the input current for different values of the noise intensity  $D$ . To this end, we measured the residence times  $T_F$  and  $T_R$  in the spiking and resting states, respectively; the transition rates were then simply defined as their inverses:  $\nu_X = 1/T_X$ . The rates for three different noise intensities are plotted in Fig. 5(a), in which the circles represent the transition rate out of the spiking state,  $\nu_F$ , and the squares indicate the transition rate out of the resting state,  $\nu_R$ . As the bias current increases,  $\nu_F$  drops whereas  $\nu_R$  increases. In other words, with increasing current it becomes more likely to occupy the spiking state. Higher noise fluctuations provide more “kicks” that are strong enough to overcome the potential barrier, boosting transition rates in general.

The effective transition rates in combination with the two-state theory capture the Fano factor and diffusion coefficients over a wide range of input currents; this is shown for the model close to the saddle-node bifurcation in Fig. 5(b). This agreement demonstrates that the firing-rate bistability is the main source of deviations from Poisson statistics, i.e., from  $F = 1$ .

The same kind of analysis (extraction of effective potential barriers from simulation data) can be carried out for the model setting close to the Andronov-Hopf bifurcation, in which case the corresponding two-state theory also captures the Fano factor and diffusion coefficient rather well [40].

#### IV. CONSEQUENCES FOR SIGNAL TRANSMISSION

We now explore how the observed giant spike-count diffusion impacts the transmission of a weak and slow signal. Specifically, we change in Eq. (1) from a constant input

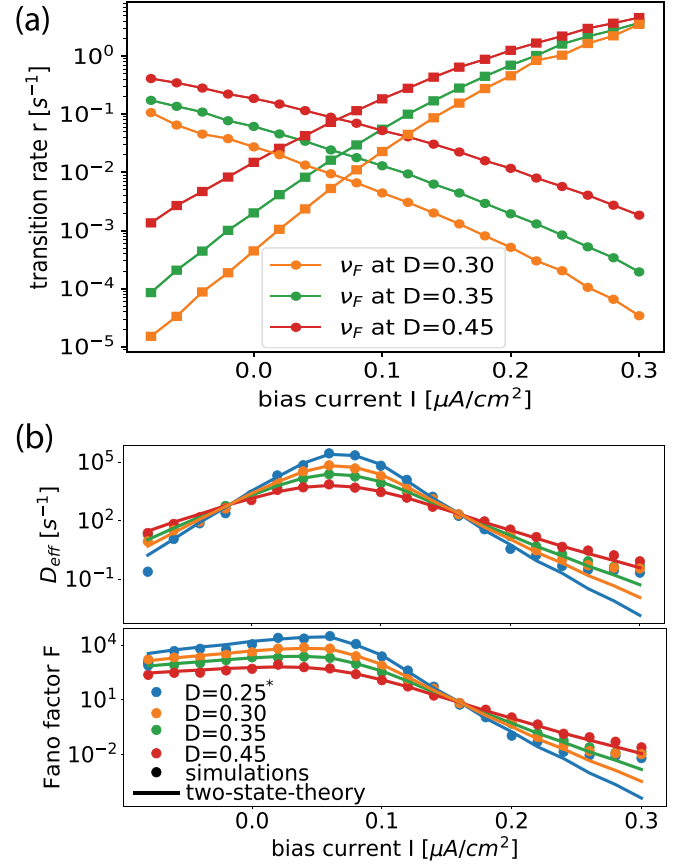


FIG. 5. Two-state theory for the  $I_{Na,p} + I_K$  model close to the saddle-node bifurcation. (a) Transition rates between spiking and resting states as the bias current is increased. A larger bias favors the spiking state, as shown by higher  $\nu_R$  (squares) and lower  $\nu_F$  (circles), while larger noise intensities  $D$  result in faster overall transition rates. (b) Comparison between measured values of  $D_{\text{eff}}$  and  $F$  (circles) and two-state theory (lines). For  $D = 0.25$ , the two-state theory was extrapolated from the other transition rates, but still showed excellent agreement with the simulations up to  $I = 0.2$ .

current  $I$  to one that is periodically modulated, i.e.,  $I \rightarrow I + \varepsilon \cos(2\pi f_s t)$ . We measure the spike train's Fourier transform over a time window  $T$ ,  $\tilde{x}(f)$ , and, by averaging over many realizations, its power spectrum  $S(f) = \langle |\tilde{x}|^2 \rangle / T$  (see Fig. 6 for two examples). The signal-to-noise ratio (SNR) is then obtained by dividing the signal-induced ac peak at the driving frequency  $f_s$  by the noise floor [41] (red lines in Fig. 6). For a weak and slow signal, the peak is given in terms of the susceptibility at zero frequency (the slope of the transfer function, i.e., the derivative of the firing rate with respect to input current), the driving amplitude  $\varepsilon$ , and the measuring time window  $T$  [42]. Furthermore, the noise floor can be approximated by the spike train power spectrum at zero frequency without the driving, which is related to the spike-count diffusion coefficient  $S(f \rightarrow 0) = 2D_{\text{eff}}$ . Hence, we arrive at the following expression for the SNR [43]:

$$\text{SNR} = \frac{\varepsilon^2 T |dr/dI|^2}{8D_{\text{eff}}}, \quad (5)$$

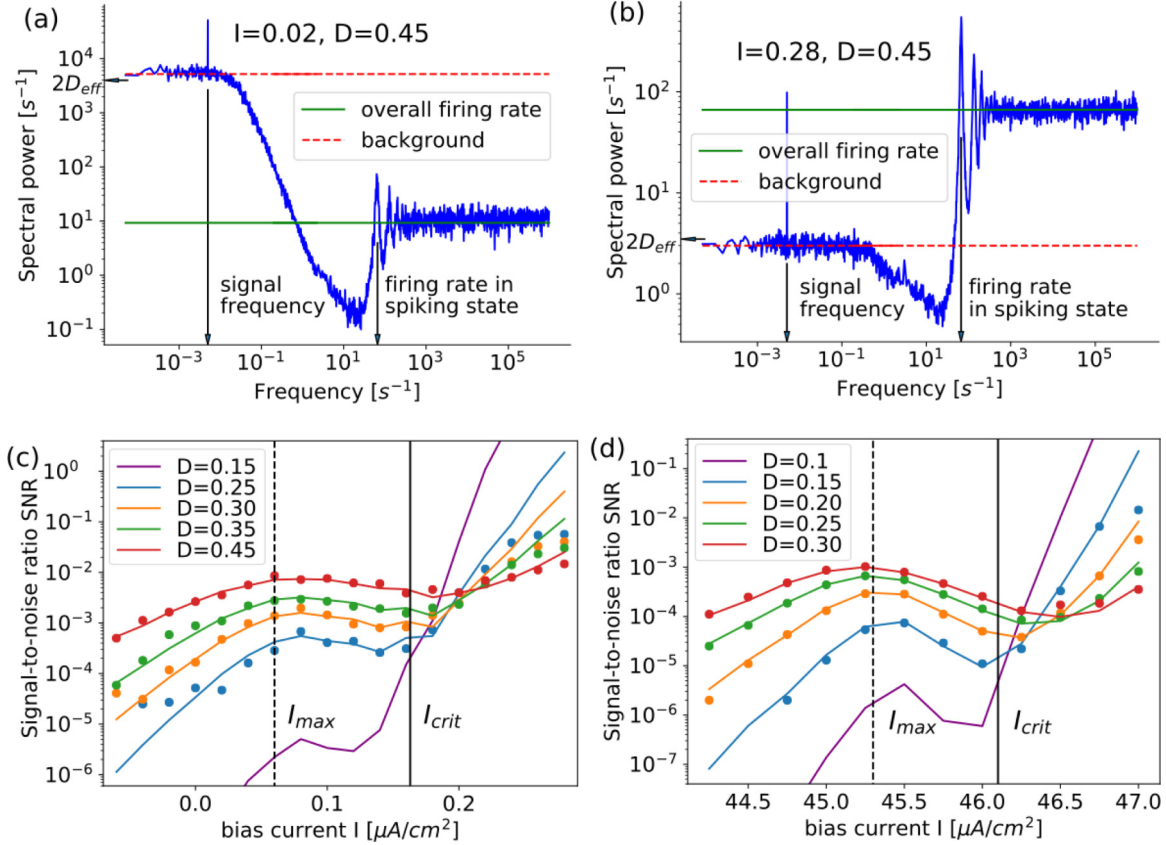


FIG. 6. Power spectra (a),(b) and signal-to-noise ratios (c),(d) of the  $I_{Na,p} + I_K$  model. Power spectra for a weak (a) and a strong (b) input current for the system close to the saddle node reveal ac peaks at the driving frequency (here  $f_s = 5 \times 10^{-3}$  Hz); low- [ $S(f \rightarrow 0) = D_{\text{eff}}$ ] and high-frequency limits [ $S(f \rightarrow \infty) = r$ ] are indicated. The measured SNRs for the system close to the saddle-node bifurcation [symbols in (c)] or close to the Andronov-Hopf bifurcation [symbols in (d)] are compared to the approximation resulting from the two-state theory (solid lines). Signal frequencies and amplitudes  $f_s = 5 \times 10^{-3}$  Hz and  $\varepsilon = 0.01 \mu\text{A}/\text{cm}^2$  for the data in (a)–(c), and  $f_s = 10^{-2}$  Hz and  $\varepsilon = 0.05 \mu\text{A}/\text{cm}^2$  for the data in (d).

which depends on the derivative of the stationary firing rate as follows:

$$\frac{dr}{dI} = \frac{d}{dI} \left( \frac{r_F v_R}{v_R + v_F} \right) = \frac{r'_F v_R}{v_R + v_F} + \frac{r_F (v_F v'_R - v_R v'_F)}{(v_R + v_F)^2}. \quad (6)$$

Here a prime denotes the derivative with respect to  $I$ . The derivative of  $r_F$  can be obtained from simulations of the noiseless system, and the derivatives of the transition rates are given by

$$v'_X = \left( \frac{v'_{0X}}{v_{0X}} - \frac{\Delta U'_X}{D} \right) v_X$$

and can now be calculated numerically from the obtained curves as discussed above in Sec. III B.

Because the diffusion coefficient determines the low-frequency limit of the power spectrum, we see already one simple effect of the giant diffusion on the signal transmission: a high diffusion coefficient implies a strong background noise that generally lowers the SNR. However, another factor is the slope of the transfer function, i.e., the derivative of the overall firing rate with respect to the input current given above in Eq. (6), and the effect of this factor cannot be neglected.

The theory as outlined above explains the numerical observations very well even quantitatively, as seen by the lines

(theory) and symbols (simulations) in Fig. 6(c), where the SNR is shown as a function of the constant input current, i.e., our asymmetry parameter. We recall that the diffusion coefficient (determining the background noise floor) suffers a rapid drop at  $I_{\text{crit}}$ , especially if the system operates at weak noise. We thus expect to find a rapid *increase* of the SNR around this value—indeed for the  $I_{Na,p} + I_K$  model such an increase not far from  $I_{\text{crit}}$  is observed. However, the SNR also shows a pronounced maximum around  $I_{\text{max}}$  which is puzzling at first glance because at this point the diffusion coefficient possesses a maximum. Importantly, at the same time, the firing rate is at this point highly sensitive with respect to changes in the bias current, and this is the dominating effect that leads to a maximization of the SNR there. Clearly, also the stochastic resonance effect [42] is present here: deep in the bistable regime, an increase in noise intensity is beneficial for the SNR.

We can use the two-state theory to predict how the run of the curve would look for an even smaller noise intensity [purple curve in Fig. 6(c)]. For this value, a reliable estimation of the SNR from numerical simulations was not possible. We see that the dominating effect for small noise intensities is the rapid drop of background noise at the critical current, i.e., the SNR maximum around the inflec-

tion point of the firing rate becomes much lower and less prominent.

Finally, it should be emphasized that the effects discussed here do not hinge on a specific bifurcation scenario; similar curves were obtained for both parameter sets throughout the analyses. Therefore, we would expect to find the effects in higher-dimensional neuron models with a firing rate bistability, for instance in the Hodgkin-Huxley model with increased extracellular potassium concentration [44].

## V. COUNT DIFFUSION AND SNR FOR A BISTABLE NETWORK

We now consider a recently proposed network model of spiking neurons [25], undergoing stochastic transitions between a nearly quiescent state and an active state with elevated firing; this random network of excitatory and inhibitory integrate-and-fire neurons shows asynchronous irregular activity in both of its states.

Beginning in Sec. VA, we describe the neural network and the relevant parameters. We then briefly discuss how the bistability can be controlled by means of external shot-noise input and network size in Sec. VB. This aspect requires a more elaborate discussion because the external drive and the noise experienced by the neurons from the Poisson input as well as from the network itself are intertwined, and therefore they cannot be altered independently as in the single-neuron case. In Sec. VC, we show that the spike-count diffusion and the SNR of the network display the same behavior as for the bistable neuron model. Finally, in Sec. VD we consider an alternative means of controlling the state asymmetry and noise intensity for a network of adapting neurons that leads to the same qualitative picture, which suggests that the phenomenon is rather general and does not hinge on the specific way in which the switching rates are controlled.

### A. Description of the network model

The model is a random recurrent network (fixed in-degree) of leaky integrate-and-fire neurons with Poisson random input [45,46]. Specifically, the model consists of  $N_e$  excitatory and  $N_i = \gamma N_e$  inhibitory neurons, where  $\gamma = 0.25$ , and thus the total network size is  $N = N_e(1 + \gamma)$ . The membrane potential of the  $k$ th neuron evolves according to

$$\tau_{m,\alpha} \dot{v}_k(t) = -v_k(t) + E_l + R_{m,\alpha} I_k^{\text{tot}}(t), \quad (7)$$

where  $\tau_{m,\alpha}$  is the membrane time constant, and  $\alpha = e, i$  indicates whether the  $k$ th neuron is excitatory or inhibitory ( $\tau_{m,e} = 20$  ms,  $\tau_{m,i} = 10$  ms). Note that  $\alpha$  is a function of  $k$  and not a free index. However, we do not indicate this dependence explicitly in order to simplify notation. Furthermore,  $E_l$  is the resting potential,  $R_{m,\alpha}$  is the membrane resistance, and  $I_k^{\text{tot}}$  is the total input current. The membrane resistance is  $R_{m,\alpha} = \tau_{m,\alpha}/C_m$  with membrane capacitance  $C_m = 1$  nF. If all voltages are measured with respect to the resting potential, then we can set  $E_l = 0$ . Whenever the voltage reaches the threshold value  $v_\theta = 20$  mV, the neuron emits a spike and the voltage is reset and clamped at  $v_r = 10$  mV for an absolute refractory period of  $\tau_{\text{ref}} = 2$  ms. All spikes emitted from a

neuron constitute its output spike train

$$x_k(t) = \sum_n \delta(t - t_{k,n}), \quad (8)$$

where  $\delta(t)$  is the Dirac delta function, and the  $n$ th spike time of the  $k$ th neuron is denoted by  $t_{k,n}$ .

The total input current  $I_k^{\text{tot}}(t)$  is composed of two terms,  $I_k^{\text{rec}}$  and  $I_k^{\text{ext}}$ , which model the recurrent and external inputs, respectively:

$$R_{m,\alpha} I_k^{\text{tot}}(t) = R_{m,\alpha} [I_k^{\text{rec}}(t) + I_k^{\text{ext}}(t)]. \quad (9)$$

The recurrent input is a sum over spike trains from the network,

$$I_k^{\text{rec}}(t) = \frac{\tau_{m,\alpha} J_\alpha}{R_{m,\alpha}} \left[ \sum_{j \in \mathcal{P}_e(k)} x_j(t - D_{kj}) - g_\alpha \sum_{\ell \in \mathcal{P}_i(k)} x_\ell(t - D_{k\ell}) \right], \quad (10)$$

where the presynaptic excitatory neighbors of neuron  $k$ ,  $\mathcal{P}_e(k)$ , are a random selection of  $C_e = 1000$  excitatory neurons, and  $\mathcal{P}_i(k)$  is a random selection of  $C_i = \gamma C_e = 250$  inhibitory neurons; self-connections are excluded. The connection probability is almost independent of the cell type and is  $p_{c,ee} = C_e/(N_e - 1) \approx p_{c,ei} = p_{c,ie} = C_i/N_i \approx p_{c,ii} = C_i/(N_i - 1) \approx C/N$ , where  $C = C_e + C_i$  is the total number of recurrent inputs per neuron. The coupling efficacy is governed by the synaptic weights,  $J_e = 0.2$  mV (from excitatory onto excitatory neurons) and  $J_i = 0.34$  mV (from excitatory onto inhibitory neurons), which are amplified by the respective factor  $g_e = g_i = 4$  for inhibitory synapses. The transmission delays  $D_{kj}$  ( $D_{k\ell}$ ) are drawn once for each neuron pair from an exponential distribution with mean  $D_{\text{ex}} = 20$  ms ( $D_{\text{inh}} = 10$  ms) if the presynaptic neuron is excitatory (inhibitory).

The external input term for the  $k$ th neuron is a sum of  $C_{\text{ext}} = 1000$  independent Poisson spike trains, each with a constant rate  $r_{\text{ext}}$ ,

$$I_k^{\text{ext}}(t) = \frac{\tau_{m,\alpha} J_\alpha}{R_{m,\alpha}} \sum_{i=1}^{C_{\text{ext}}} \sum_l \delta(t - t_{k,i,l}), \quad (11)$$

where the  $t_{k,i,l}$  indicate the firing times. Inputs  $I_k^{\text{ext}}(t)$  and  $I_{k'}^{\text{ext}}(t)$  to different neurons ( $k \neq k'$ ) are statistically independent; they all possess the same postsynaptic efficacy on a neuron in a population as an excitatory neuron from the network, that is,  $J_\alpha$ .

Equations are integrated with an Euler time scheme and time step  $\Delta t = 0.01$  ms. In each of the 100 trials, the network is simulated first for  $T_{\text{init}} = 0.1$  s, which is discarded from the analysis. Spikes are then recorded for a time window  $T = 1000$  s. (For the population with  $N_e = 3000$ , it was necessary to run the trials for  $T = 2000$  s such that an adequate number of transitions between states occurred.)

With this choice of parameters, the global activity shows bistability, as made clear by the raster plot seen in Fig. 7(a). Indeed, the network jumps between an active (“up”) state and a quiescent (“down”) state. This kind of firing regime is often observed in cortical networks during sleep, anesthetized, or idling states [47,48]. In the down-state, the network is almost

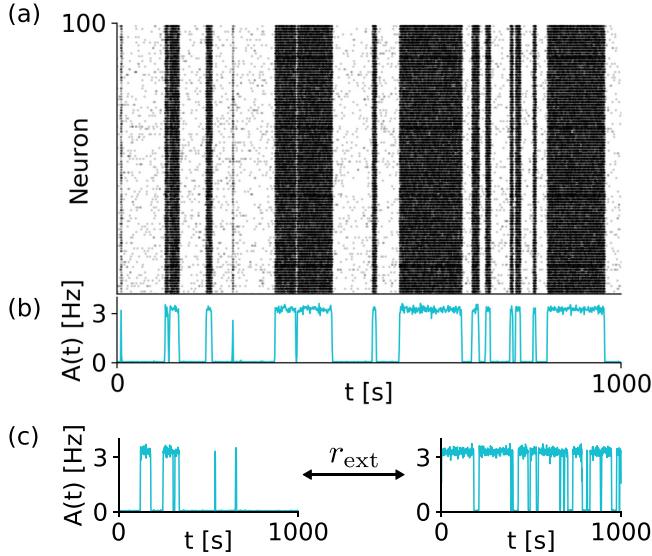


FIG. 7. Firing rate bistability in the network model. (a) Raster plot from a single trial for 100 randomly selected excitatory neurons. (b) Network firing rate  $A(t) = 1/N_e \sum_k x_k \star B(t)$ , where  $x_k(t)$  is the spike train of the  $k$ th neuron given by (8),  $B(t)$  is a normalized box function with length 1 s, and  $\star$  indicates convolution. (c) The probability of being in the active state can be adjusted via the external input rate (cf. Fig. 1). Parameters are as follows:  $N_e = 2000$ ,  $T = 1000$  s,  $\varepsilon = 0$ ,  $r_{\text{ext}} = 3.7162$  Hz (b);  $r_{\text{ext}} = 3.7100$  Hz (c, left);  $r_{\text{ext}} = 3.7225$  Hz (c, right).

silent, while the up-state is characterized by sustained, asynchronous irregular firing with an average rate (per neuron) of  $\approx 3$  Hz [Fig. 7(b)]. For a detailed discussion of this bistability, see Ref. [25].

To measure the signal-to-noise ratio (SNR), a slow and weak periodic current

$$I_{\text{sig},\alpha}(t) = \frac{\varepsilon}{R_{m,\alpha}} \cos(2\pi f_s t) \quad (12)$$

is injected into each neuron (added to the currents in eq. (9)), where  $\varepsilon/R_{m,\alpha} = 0.1$  mV and  $f_s = 0.01$  Hz. The measures computed in the following use the sum of all spikes fired by the excitatory population.

### B. Bistability and the role of parameters

Transitions between the two states are caused by the interplay of the external random input received by each neuron with the recurrent network dynamics. Note that the effective input noise received by each neuron in the network depends not only on the choice of parameters, but also on the current state of the network. Hence, a separate control of transition rates and state asymmetry is not as straightforward as in the case of a single neuron and cannot be achieved by varying a single parameter. One simple way of manipulating the asymmetry is changing the rate of the external input, as demonstrated in Fig. 7(c): intuitively, a stronger excitatory drive makes the active state more likely. Because the active state's average rate is affected little by this transition in external input, the shift in state probability with input is also reflected in the network's average rate curve in Fig. 8(a),

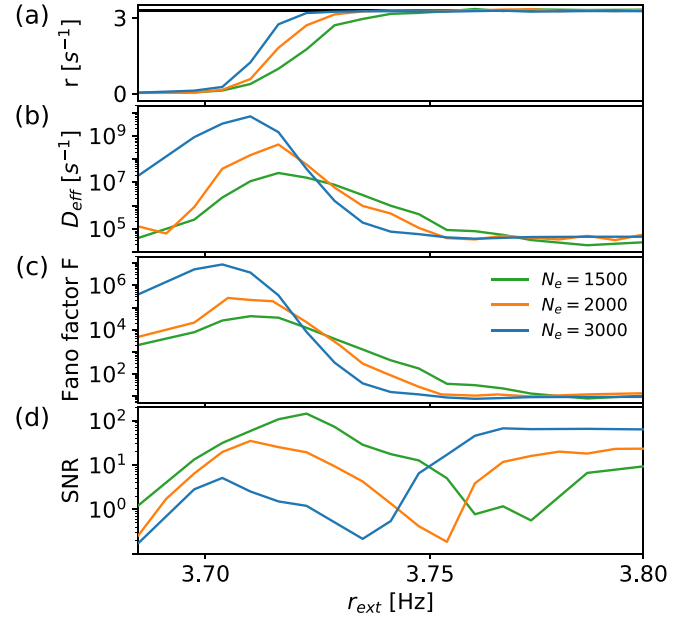


FIG. 8. Count statistics and SNR of the excitatory neurons of a recurrent network. From top to bottom: average firing rate, effective diffusion coefficient, Fano factor, and signal-to-noise ratio for periodic stimulation. All statistics are plotted as functions of the rate  $r_{\text{ext}}$  of the excitatory Poissonian input spikes and for different network sizes  $N_e$  as indicated; other parameters:  $T = 1000$  s (for  $N_e = 3000$ ,  $T = 2000$  s),  $\Delta t = 0.01$  ms,  $N_i = 0.25N_e$ ,  $v_\theta = 20$  mV,  $v_r = 10$  mV,  $\tau_{m,e} = 20$  ms,  $\tau_{m,i} = 10$  ms,  $\tau_{\text{ref}} = 2$  ms,  $C_e = C_{\text{ext}} = 1000$ ,  $C_i = 250$ , exponentially distributed synaptic delays with averages  $D_{\text{ex}} = 20$  ms and  $D_{\text{inh}} = 10$  ms,  $g_e = g_i = 4$ ,  $J_e = 0.2$  mV (no autapses),  $J_i = 0.34$  mV,  $\varepsilon = 0.1$  mV,  $f_s = 0.01$  Hz.

where a rate near 3 Hz indicates the network occupying the active state more often.

To draw a comparison with the single neuron, for which the noise level was changed to manipulate the switching rates between states (without affecting the state probabilities), the total network size was varied while keeping the number of connections per neuron fixed. In this way, the connection probability changes according to  $p_c = C/N$ , which means that larger networks are more sparsely connected. The connection probability has an impact on the cross-correlations in the network [46,49–51], which in turn strongly influence the internally (autonomously) generated part of the network noise. Each neuron in the network is subject to both an external noise source (a sum of  $C_{\text{ext}}$  independent Poisson spike trains) and an internally generated noise source, i.e., the superposition of  $C$  quasirandom input spike trains. The internally generated noise depends not only on cross-correlations and all network parameters, *but also on the network state*, since the total input firing rate that each neuron receives is very different in the two states. For this reason, any change in the network parameters that alters the effective noise intensity is likely to have a different impact on the stability of the two states and must be compensated for in some way if the symmetry of the transition rates is to be preserved. Hence, although the network size can be used to manipulate switching rates, the effect is not equal on the two states, such that the inflection point (i.e., where the

switching probability is equal to 1/2) is also slightly shifted, as seen in Fig. 8(a).

### C. Giant count diffusion and SNR for the bistable network

The previous subsections clearly showed that the separation of state asymmetry from the noise level achieved by changes in the external input and recurrent connection probability is not strict, because, for instance, the Poisson trains also contribute to the noise in the system. Yet, if we plot the diffusion coefficient [Fig. 8(b)] and Fano factor [Fig. 8(c)] of the population's spike count as functions of the external rate, we see a very similar behavior as in the single-neuron case: both functions go through maxima that are roughly attained where the firing rate [Fig. 8(a)] has its inflection point, and the maxima are more pronounced if we reduce the intrinsic noise by increasing the network size.

If we drive the network with a common cosine stimulus, the SNR for this signal [Fig. 8(d)] exhibits the same shape we have already discussed for the single-neuron case [cf. Fig. 6(c)]: a local maximum at the point of maximized diffusion, a minimum at intermediate rate, and a pronounced increase beyond the point of critical asymmetry. Another robust observation is that with decreasing noise, the local maximum shrinks and the increase at high input rates becomes stronger.

In the next section, an alternative way to manipulate transition rates is discussed. Importantly, the qualitative shape of all curves is conserved, which suggests that the main effect discussed in this study does not depend on a specific mechanism. It requires only that the system is bistable with long residence times in each state and that the asymmetry of those states can be controlled.

### D. Model with spike-frequency adaptation

Many excitatory pyramidal neurons in the neocortex display spike-frequency adaptation [52,53]. A simple and well-established model for this biological mechanism is a self-inhibition current  $a_k(t)$  modifying the input current (9) for excitatory neurons as follows:

$$R_{m,e}I_k^{\text{tot}}(t) = R_{m,e}[I_k^{\text{rec}}(t) + I_k^{\text{ext}}(t) - a_k(t)]. \quad (13)$$

The adaptation variable obeys [53–55]

$$\tau_a \dot{a}_k(t) = -a_k(t) + \tau_a \Delta_a x_k(t), \quad (14)$$

in which the adaptation variable is driven by the neuron's own spike train, Eq. (8). In (14),  $\Delta_a$  is the adaptation strength and  $\tau_a = 500$  ms is the adaptation-current relaxation time. The asymmetry in the state probabilities was controlled, as for the nonadaptive network, by changing the input rate of the external Poisson input. Here, however, we chose a reference value of the external shot-noise input,  $\hat{r}_{\text{ext}} = 0.7445 \times r_\theta$ , where  $r_\theta = v_\theta / (\tau_{m,e} J_e C_e)$ , and we varied the input rate of each external input spike by  $\Delta r_{\text{ext}} = \Delta \mu_{\text{eff}} / (\tau_{m,e} J_e C_{\text{ext}})$ . This change in the external input rate corresponds to a change in the mean input by  $\Delta \mu_{\text{eff}}$  with respect to the reference value. In other words, the external input rate corresponding to a given  $\Delta \mu_{\text{eff}}$  is  $\hat{r}_{\text{ext}} + \Delta \mu_{\text{eff}} / (\tau_{m,e} J_e C_{\text{ext}})$ . In this subsection, simulation results are plotted as a function of  $\Delta \mu_{\text{eff}}$ .

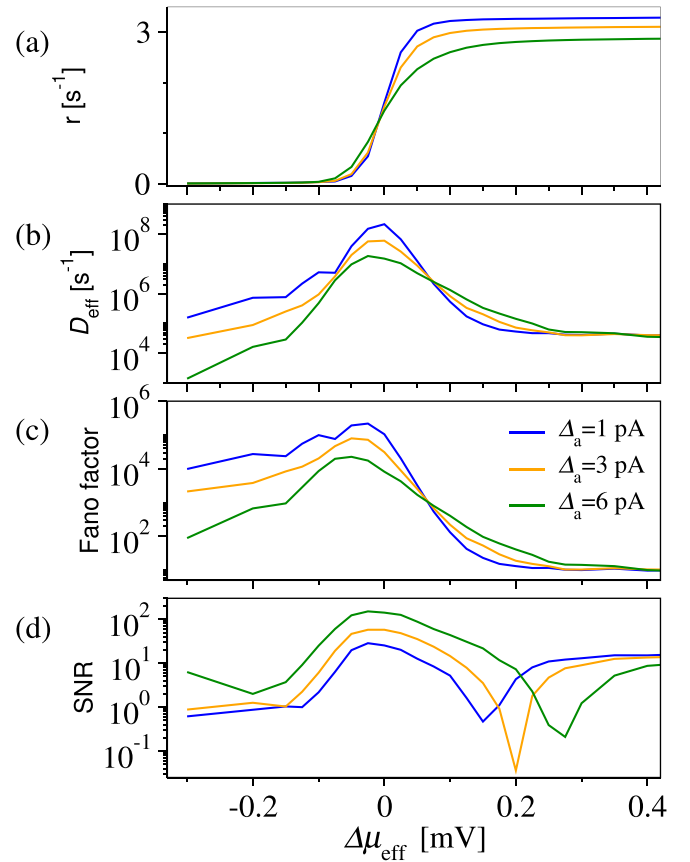


FIG. 9. Giant spike-count diffusion and consequences for the SNR in a network model with spike-frequency adaptation. From top to bottom: average single-neuron firing rate (a), network spike-count diffusion coefficient  $D_{\text{eff}}$  (b), network spike-count Fano factor (c), and SNR (d) as functions of the mean external effective input  $\Delta \mu_{\text{eff}}$ . The effective noise is controlled by changing the spike-frequency adaptation parameter  $\Delta_a$ . The resting potential  $E_l(\Delta_a)$  for each value of  $\Delta_a$  is chosen such that the two states are equally probable for  $\Delta \mu_{\text{eff}} = 0$ . Parameters:  $\Delta t = 0.1$  ms,  $f_s = 0.1$  Hz. All other parameters are the same as for the nonadaptive network in Fig. 8. The statistics shown here were calculated from the spike trains of the entire network, as opposed to only the excitatory population output used for the nonadaptive network.

As a more substantial difference from the nonadaptive case, instead of changing the network size and sparsity, the transition rate between up- and down-states was manipulated by changing the strength of the spike-frequency adaptation  $\Delta_a$ , which in the cortex can vary according to the cell type even within the same region [52]. Increasing  $\Delta_a$  decreases the mean lifetime of up-states more than that of down-states. To ensure that up- and down-states are equally probable for  $\Delta \mu_{\text{eff}} = 0$ , the resting potential of each neuron was shifted by a suitable value  $E_l(\Delta_a)$ , found empirically.

Figure 9(a) shows the average firing rate as a function of  $\Delta \mu_{\text{eff}}$  for three values of  $\Delta_a$ . As stated above, these two parameters manipulate state asymmetry and switching rates, respectively, and they play a similar role as the bias input current and channel noise in the single-neuron case. Although for  $\Delta \mu_{\text{eff}} = 0$  the up- and down-states are equally likely, the firing rate in the up-state slightly depends on  $\Delta_a$ , so



that the three curves do not intersect exactly at the same point.

The spike-count diffusion coefficient  $D_{\text{eff}}$  (computed here from all spikes fired by the entire network) displays a large maximum when the up- and down-states are equiprobable [Fig. 9(b)]. For  $\Delta\mu_{\text{eff}} > 0$ , the diffusion coefficient drops drastically. The decrease is faster for smaller values of  $\Delta_a$  (which correspond to lower effective transition rates). All curves intersect at the same value, which can be seen as a critical value of the mean input (with respect to the operation point), as in the single neuron model. Although (as explained in the previous paragraph) by design the firing rate curves in Fig. 9(a) almost perfectly intersect at  $\Delta\mu_{\text{eff}} = 0$ , this does not prescribe the behavior of the other statistics, such as  $D_{\text{eff}}$ . More specifically, it does not imply the intersection at the critical point, which is a result of the system's behavior. Well above the critical value, the decrease of  $D_{\text{eff}}$  tends to saturate due to the intrinsic firing variability of the up-state, which sets a lower boundary for the decrease of the spike-count diffusion. The Fano factor shows a similar behavior [Fig. 9(c)].

Finally, we inject a weak and slow periodic current into each neuron of the network according to (12) with  $f_s = 0.1$  Hz and measure the SNR, defined as in the single-neuron case and shown in Fig. 9(d). All SNR curves display the same qualitative N-shaped behavior seen for the single-neuron and nonadaptive network cases. Specifically, we observe a large maximum where the spike-count giant diffusion occurs, a sharp decrease happens in the vicinity of the critical input, and there is a clear growing trend above the critical value. Note that the saturation of  $D_{\text{eff}}$  sets a limit on the growth of the SNR. Using a larger, sparser network would reduce the intrinsic variability of the network's firing rate (as seen in Fig. 8), which depends in general on the network size and how the weights are scaled [51,56].

## VI. CONCLUSIONS

Measuring the linear response to a weak periodic stimulus has been an experimental standard for many decades (see, e.g., [57,58]). Changing the operation point of the neuron (i.e., the constant part of the injected current) is likewise common in the field. Our findings predict that an experimenter measuring the SNR in a neuron with a comparatively low noise level would find a drastic increase at  $I_{\text{crit}}$ . Nothing in the firing rate curve (the transfer function) would hint at why at this value anything special could happen. Our analogy with the mechanical transport model and the diffusion problem provides an instructive explanation: an increase in current during spontaneous activity leads to a strong drop of the diffusion coefficient because at this point the system becomes sufficiently asymmetric (see [3]). As the diffusion coefficient of the spontaneous activity controls the background noise level in the case of driven activity [42], a strong decrease of the

diffusion coefficient accompanies a strong increase of the SNR. Particularly at small noise levels [cf. the purple curve in Fig. 6(c)], our theory predicts that this strong drop of the diffusion coefficient (appearing in the denominator of the SNR) will outweigh the decrease in the numerator, which is due to the bias-current dependence of the slope factor.

At the network level, we found similar effects of the firing bistability on spike-count diffusivity and the properties of signal transmission: count diffusion and Fano factor go through several orders of magnitude when the asymmetry between the two firing states is changed, and the signal-to-noise ratio for a weak common stimulus exhibits the typical N shape (a maximum and a minimum) as a function of the external input rate. For the network, the separation into bias parameter and noise level is not as clean as in the single-neuron example if we stick to network-relevant parameters such as the constant rate of external (signal-unrelated) input spikes or the network size. However, the qualitative picture resembles what was found for the single neuron. Our results demonstrate how an external input can control the information transfer by a recurrent network, and that for larger networks variations of the SNR over orders of magnitude can emerge for rather small changes in input rates.

Our results lead to a number of challenges for future investigations. First of all, the single-neuron experiment outlined above should be performed at different levels of noise. While it does not seem to be a problem to inject *more* noise into the neuron (on top of the constant bias current and the periodic signal), to reach really low levels of noise, experimenters may have to resort to special cell types, e.g., as in [59], with apparently very low levels of intrinsic noise. Secondly, we could think of relaxing some of our conditions on the signal transmission scheme. We could generalize the setup to a nonperiodic signal (e.g., a Gaussian broadband stimulus), estimate lower bounds of the mutual information [60–62], and study this more general measure of information transmission as a function of the stimulus bandwidth. Visual cortex cells of different kinds of vertebrates have shown highly reliable spiking behavior in response to random stimuli [63,64], which might happen for bistable neurons as well. Last but not least, the implications of the found giant spike-count diffusion for the autonomous dynamics of recurrent networks is worth further exploration with respect to the emergence of slow timescales. The incorporation of bistable neurons in network models has drastic effects; it may result in a high degree of synchronization, in abrupt cessations of network activity [65,66], as well as in improving the robustness of working memory [67]. Although already tonically firing cells can show slow correlations when connected in random networks [68–71], the addition of a subpopulation of bistable cells to a recurrent network will be another source of slow processes—controlled, as we have shown here, by the mean input from external sources and from the rest of the network.

[1] B. Lindner and E. M. Nicola, *Eur. Phys. J. ST.* **157**, 43 (2008).

[2] M. Badoual, F. Jülicher, and J. Prost, *Proc. Natl. Acad. Sci. (USA)* **99**, 6696 (2002).

- [3] B. Lindner and E. M. Nicola, *Phys. Rev. Lett.* **101**, 190603 (2008).
- [4] H. Risken, *The Fokker-Planck Equation* (Springer, Berlin, 1984).
- [5] H. Vollmer and H. Risken, *J. Phys. B* **52**, 259 (1983).
- [6] P. Jung and H. Risken, *Z. Phys. B* **54**, 357 (1984).
- [7] B. Lindner and I. M. Sokolov, *Phys. Rev. E* **93**, 042106 (2016).
- [8] G. Costantini and F. Marchesoni, *Europhys. Lett.* **48**, 491 (1999).
- [9] K. Lindenberg, A. M. Lacasta, J. M. Sancho, and A. H. Romero, *New J. Phys.* **7**, 29 (2005).
- [10] I. G. Marchenko and I. I. Marchenko, *Europhys. Lett.* **100**, 50005 (2012).
- [11] J. Jalife and C. Antzelevitch, *Science* **206**, 695 (1979).
- [12] Y. Loewenstein, S. Mahon, P. Chadderton, K. Kitamura, H. Sompolinsky, Y. Yarom, and M. Häusser, *Nat. Neurosci.* **8**, 202 (2005).
- [13] J. Hounsgaard and O. Kiehn, *J. Physiol.* **414**, 265 (1989).
- [14] E. Marder, L. Abbott, G. Turrigiano, Z. Liu, and J. Golowasch, *Prec. Natl. Acad. Sci. (USA)* **93**, 13481 (1996).
- [15] P. Fuentealba, I. Timofeev, M. Bazhenov, T. Sejnowski, and M. Steriade, *J. Neurophysiol.* **93**, 294 (2005).
- [16] M. Steriade, A. Nunez, and F. Amzica, *J. Neurosci.* **13**, 3266 (1993).
- [17] C. C. H. Petersen, T. T. G. Hahn, M. Mehta, A. Grinvald, and B. Sakmann, *Proc. Natl. Acad. Sci. (USA)* **100**, 13638 (2003).
- [18] J. F. A. Poulet, L. M. J. Fernandez, S. Crochet, and C. C. H. Petersen, *Nat. Neurosci.* **15**, 370 (2012).
- [19] A. Luczak, P. Bartho, and K. D. Harris, *J. Neurosci.* **33**, 1684 (2013).
- [20] T. A. Engel, N. A. Steinmetz, M. A. Gieselmann, A. Thiele, T. Moore, and K. Boahen, *Science* **354**, 1140 (2016).
- [21] F. Droste and B. Lindner, *eNeuro* **4**, e0282 (2017).
- [22] D. Holcman and M. Tsodyks, *PLoS Comput. Biol.* **2**, e23 (2006).
- [23] A. Destexhe, *J. Comput. Neurosci.* **27**, 493 (2009).
- [24] D. Jercog, A. Roxin, P. Barthó, A. Luczak, A. Compte, and J. de la Rocha, *eLife* **6**, e22425 (2017).
- [25] E. M. Tartaglia and N. Brunel, *Sci. Rep.* **7**, 11916 (2017).
- [26] G. Ermentrout and D. Kleinfeld, *Neuron* **29**, 33 (2001).
- [27] S. di Santo, R. Burioni, A. Vezzani, and M. A. Muñoz, *Phys. Rev. Lett.* **116**, 240601 (2016).
- [28] V. Buendía, S. di Santo, P. Villegas, R. Burioni, and M. A. Muñoz, *Phys. Rev. Res.* **2**, 013318 (2020).
- [29] E. M. Izhikevich, *Dynamical Systems in Neuroscience: The Geometry of Excitability and Bursting* (The MIT Press, Cambridge, MA and London, UK, 2007).
- [30] P. J. Thomas and B. Lindner, *Phys. Rev. Lett.* **113**, 254101 (2014).
- [31] M. P. Nawrot, C. Boucsein, V. R. Molina, A. Riehle, A. Aertsen, and S. Rotter, *J. Neurosci. Methods* **16**, 374 (2008).
- [32] K. Rajdl, P. Lansky, and L. Kostal, *Front. Comput. Neurosci.* **14**, 569049 (2020).
- [33] C. Van den Broeck, *Physica A* **168**, 677 (1990).
- [34] C. Touya, T. Schwalger, and B. Lindner, *Phys. Rev. E* **83**, 051913 (2011).
- [35] M. N. Shadlen and W. T. Newsome, *J. Neurosci.* **18**, 3870 (1998).
- [36] M. Churchland *et al.*, *Nat. Neurosci.* **13**, 369 (2010).
- [37] F. Gabbiani and S. J. Cox, *Mathematics for Neuroscientists* (Academic, Amsterdam, 2017).
- [38] A. Riehle, T. Brochier, M. Nawrot, and S. Grün, *Front Neural Circuit* **12**, 52 (2018).
- [39] J.-H. Schleimer, J. Hesse, S. A. Contreras, and S. Schreiber, *Phys. Rev. E* **103**, 012407 (2021).
- [40] R. Kullmann, Master's thesis, Humboldt Universität zu Berlin (2020).
- [41] S. Fauve and F. Heslot, *Phys. Lett. A* **97**, 5 (1983).
- [42] L. Gammaitoni, P. Hänggi, P. Jung, and F. Marchesoni, *Rev. Mod. Phys.* **70**, 223 (1998).
- [43] B. Lindner, *Coherence and Stochastic Resonance in Nonlinear Dynamical Systems* (Logos-Verlag, Berlin, 2002).
- [44] J. Rinzel, *Fed. Proc.* **44**, 2944 (1985).
- [45] D. J. Amit and N. Brunel, *Cereb. Cortex* **7**, 237 (1997).
- [46] N. Brunel, *J. Comput. Neurosci.* **8**, 183 (2000).
- [47] A. Renart, J. de la Rocha, P. Bartho, L. Hollender, N. Parga, A. Reyes, and K. D. Harris, *Science* **327**, 587 (2010).
- [48] K. D. Harris and A. Thiele, *Nat. Rev. Neurosci.* **12**, 509 (2011).
- [49] S. Ostojic, N. Brunel, and V. Hakim, *J. Neurosci.* **29**, 10234 (2009).
- [50] J. Trousdale, Y. Hu, E. Shea-Brown, and K. Josic, *PLoS Comput. Biol.* **8**, e1002408 (2012).
- [51] D. Bernardi and B. Lindner, *Phys. Rev. Lett.* **118**, 268301 (2017).
- [52] M. Beierlein, J. R. Gibson, and B. W. Connors, *J. Neurophysiol.* **90**, 2987 (2003).
- [53] J. Benda and A. V. M. Herz, *Neural Comput.* **15**, 2523 (2003).
- [54] T. Schwalger and B. Lindner, *Front. Comp. Neurosci.* **7**, 7164 (2013).
- [55] D. Bernardi, G. Doron, M. Brecht, and B. Lindner, *PLOS Comput. Biol.* **17**, e1007831 (2021).
- [56] D. Bernardi and B. Lindner, *Phys. Rev. E* **99**, 032304 (2019).
- [57] B. W. Knight, *J. Gen. Physiol.* **59**, 767 (1972).
- [58] T. Tchumatchenko, A. Malyshev, F. Wolf, and M. Volgushev, *J. Neurosci.* **31**, 12171 (2011).
- [59] Z. F. Mainen and T. J. Sejnowski, *Science* **268**, 1503 (1995).
- [60] F. Rieke, D. Warland, R. de Ruyter van Steveninck, and W. Bialek, *Spikes: Exploring the Neural Code* (MIT Press, Cambridge, MA, 1996).
- [61] N. Brunel and J. P. Nadal, *Neural Comput.* **10**, 1731 (1998).
- [62] S. Voronenko and B. Lindner, *Biol. Cybern.* **112**, 523 (2018).
- [63] G. Buracas, A. Zador, M. DeWeese, and T. Albright, *Neuron* **20**, 959 (1998).
- [64] P. Kara, P. Reinagel, and R. Reid, *Neuron* **27**, 635 (2000).
- [65] M. Uzuntarla, J. Torres, A. Calim, and E. Barreto, *Neural Netw.* **110**, 131 (2018).
- [66] A. V. Andreev, N. S. Frolov, A. N. Pisarchik, and A. E. Hramov, *Phys. Rev. E* **100**, 022224 (2019).
- [67] M. Camperi and X.-J. Wang, *J. Comput. Neurosci.* **5**, 383 (1998).
- [68] A. Litwin-Kumar and B. Doiron, *Nat. Neurosci.* **15**, 1498 (2012).
- [69] S. Ostojic, *Nat. Neurosci.* **17**, 594 (2014).
- [70] S. Wieland, D. Bernardi, T. Schwalger, and B. Lindner, *Phys. Rev. E* **92**, 040901(R) (2015).
- [71] R. Pena, S. Vellmer, D. Bernardi, A. Roque, and B. Lindner, *Front. Comp. Neurosci.* **12**, 9 (2018).